SNO-STR-95-052

University of Waterloo
Faculty of Science

SNO Calibration Source Optimization

AECL Research
NCMS Branch
Chalk River Laboratories
Chalk River, Ontario

Kevin Murnaghan
ID 91158969
3A Applied Physics
August 28, 1995

Table of Contents

List of Tables

List of Figures

Summary

Several types of calibration devices have been proposed for the Sudbury Neutrino Observatory (SNO). The use of ^{17}N and ^{16}N gas as calibration sources has been successfully investigated previously.

The optimum dimensions of such a calibration system were determined using a computer program, GOPTSTP.

A study of gas flow in teflon capillary tubing was perfomed to determine the accuracy of theoretical predictions. From this study a model was developed which fits within theory.

Conclusions

^{16}N and ^{17}N can be used as calibration sources for SNO using the same set of target and decay chambers.

A verified model for gas flow in teflon capillary has been developed which should be useful for further work.

Recommendations

The final design of calibration system components, including scale diagrams, can be completed when the design has been completed and evaluated by the collaboration.

A similar optimization should be done for the use of ^{8}Li as the target.

1. Introduction

The Sudbury Neutrino Observatory (SNO) was designed to study the differences currently experienced between observations and theoretical predictions of solar neutrino behaviour. At present other detectors observe a significant deficit in the flux of solar neutrinos. This deficit may be caused by the sun's core being cooler than present theories suggest from surface observations. Observing neutrinos from the sun allows measurements to be made of the present solar core conditions.

Neutrinos are fundamental particles that are found in nature. They are generated in star cores through the fusion process. There are three flavours of neutrinos: the electron neutrino, the tau neutrino and the mu neutrino. If a neutrino has any mass it is expected to be small. If they have mass they may be capable of oscillating between flavours. Neutrinos are only influenced by the weak force so they pass through matter with little interaction, making them difficult to detect. A neutrino has a 1 in 10^{10} chance of an interaction in passing through the earth. {6}

The solar neutrino energy spectrum will be measured to determine if vacuum or matter-enhanced neutrino oscillations occur. These measurements are possible since SNO is sensitive to all types of neutrinos. SNO can differentiate between electron neutrinos and the total flux of flavour independent neutrinos. SNO is expected to observe fifteen solar neutrinos per day. Time variations in the solar neutrino flux will be possible because of the high event rate of SNO. {5}

SNO is located in Inco's Creighton Mine near Sudbury. A 22 m diameter, 30 m high, barrel shaped cavern has been excavated 2070 meters underground to house the detector. The detector consists of 1000 tonnes of 99.85% enriched heavy water enclosed within a 12 m diameter

acrylic vessel. The 5 cm thick acrylic vessel is partially supported and shielded by 7300 tonnes of ultra pure light water. Surrounding the acrylic vessel are 9600 20 cm photomultiplier tubes (PMTs), with light concentrators, arranged in a sphere 16 m in diameter which provide 60% photocathode coverage. The PMTs are 2.5 m away from the acrylic to provide shielding for the heavy water. The observatory is operated under clean room conditions and materials have been specially selected to reduce the background. The background limits the lowest energy measurement to around 5 MeV. {9}

1.1 Detection

The active detection component of SNO are the PMTs while heavy water is the detection medium. SNO is unique in its detection medium. The PMTs detect light within the cavity that is produced from any source. The control system records the time and location of the light events. This information is used to reconstruct the energy and direction of particle decays caused by the neutrinos. SNO is capable of observing all three types of neutrinos using three reactions. The electron neutrino flux and spectrum can be measured 2 ways, while the total neutrino flux is measured with a 3rd reaction. The anti electron neutrino flux and energy spectrum can be measured with a 4th reaction.

The charged current (CC) reaction, shown below, takes place in heavy water. The Cerenkov radiation released while the high energy electron thermalizes is detected by the PMTs.

This reaction makes the detector forty times more sensitive to electron neutrinos than other present detectors.

$$\nu_e + d \rightarrow p + p + e^- \qquad Q = -1.44\ MeV \qquad \text{(CC)}$$

The Neutral Current (NC) reaction, shown below, takes place in heavy water as well. For this reaction the neutron is the signature. The neutrons thermalize in the water and when captured generate gamma rays. The gamma rays produce relativistic electrons, mainly through Compton scattering, which give off Cerenkov radiation as they are moderated. This reaction provides a measurement of the total flux of neutrinos. The total solar ^8B neutrino production rate will be observed using the NC reaction.

$$\nu_x + d \rightarrow \nu_x + p + n \qquad Q = -2.2\ MeV \qquad \text{(NC)}$$

The neutrino electron elastic scattering (ES) reaction, shown below, takes place in both light and heavy water. This reaction is used in several detectors. This reaction is sensitive to all types of neutrinos but is dominated by the electron neutrino. The observatory expects to observe one tenth as many reactions from the ES reaction as from the CC reaction.

$$\nu_x + e^- \rightarrow \nu_x + e^- \qquad \text{(ES)}$$

The anti-neutrino charged current (ACC) reaction, shown below, occurs in heavy water. The signature of this reaction is a positron signal followed by a delayed neutron capture.

$$\bar{\nu}_e + d \rightarrow n + n + e^+ \qquad Q = -4.03\ MeV \qquad \text{(ACC)}$$

1.2 Calibrations

There are several possible calibration sources for SNO. This paper deals with the possibility of using ^{16}N and ^{17}N gas. ^{16}N decomposes by a β-decay followed by a 6.13 MeV γ-ray, which provides an absolute energy calibration. ^{17}N will be used to provide an absolute neutron capture efficiency calibration. This nuclide decays by β delayed neutron emission, these β particles can be detected to provide a tagged neutron source.

The radioactive gases can be produced with a D-T neutron generator. The ^{16}N will be generated using the $^{16}O(n,p)^{16}N$ reaction, the ^{17}N gas will be produced using $^{17}O(n,p)^{17}N$. The gas is used as both the target and carrier in these systems. An initial study of this setup has been done at Chalk River Laboratories (CRL). {8}

Figure 1.1 Calibration System Components

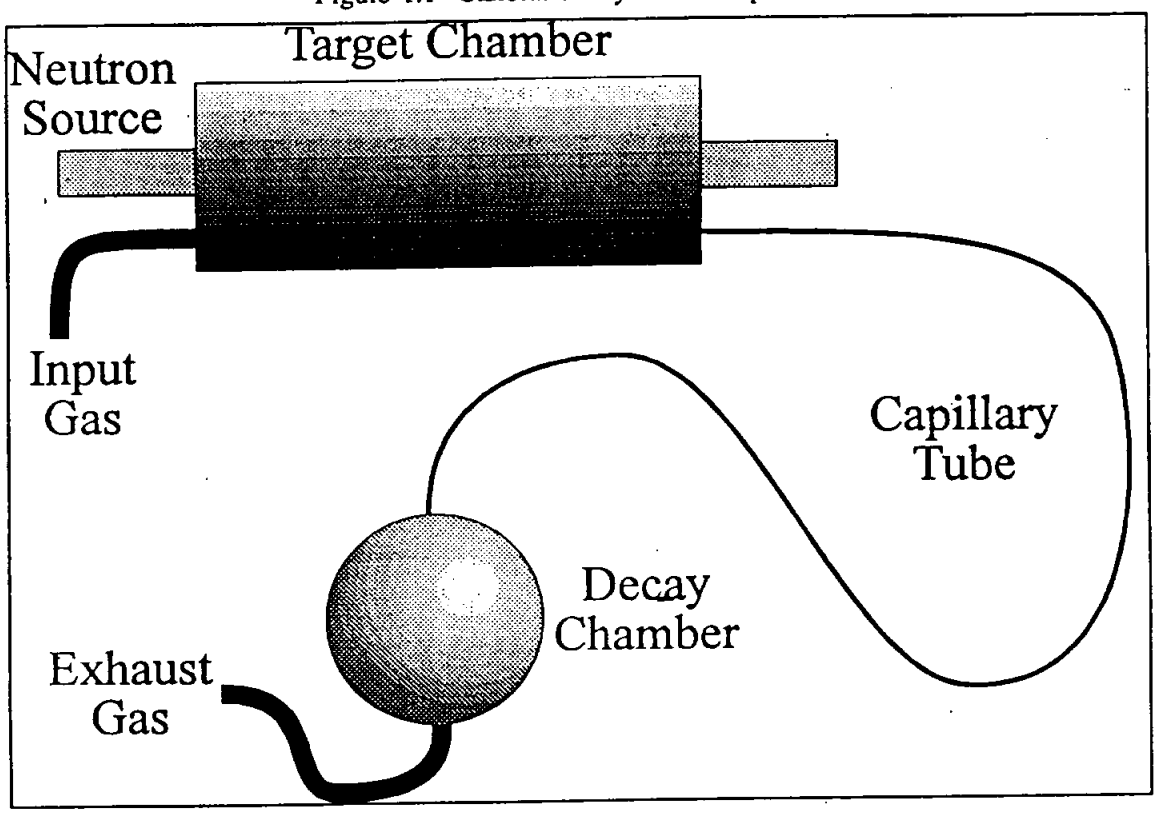

The calibration apparatus is shown in figure 1.1, above. The target chamber is cylindrical with the neutron source inserted through a centred annulus. The target chamber will be located in the Neutron Pit. The decay chamber will be located in the centre of the Acrylic Vessel for calibration and removed during normal operation. The decay chamber is spherically shaped to facilitate data analysis of the calibration data. A thin capillary tube runs between the target and decay chambers to provide rapid transport of the radioactive gas.

This apparatus could be used for many different sources using solid liquid or gas targets. An aerosol must be present in the gas if a solid target is to be used. The recoil ions from a solid target stick to the aerosol and are transported though the system. Specifically the use of ^{8}Li has been investigated for a differential energy calibration. A more accurate model is needed to predict the results of this isotope because of it's significantly shorter half life (0.838 s).

2. Theory

The production rate of the gas calibration system is dependent on the many variables as shown in table 2.1.

Table 2.1, Calibration System Variables

Name	Unit	Limit		Description
		Lower	Upper	
Ptgt	abs atm	1.25	5.00	pressure of target chamber
R1	cm	2.54	2.54	inner radius of target chamber
R2	cm	2.54	20.0	outer radius of target chamber
H	cm	1.00	25.0	length of target chamber
XX	cm	0.01	15	source offset from end of target chamber
Cl	cm	7000	7000	capillary length
Cr	cm	0.001	0.250	capillary radius
Pdec	abs atm	1.25	5.00	pressure of decay chamber
Rdec	cm	0.1	5	radius of spherical decay chamber

Several of these variables have limits associated with them. R1 has to be large enough to accommodate the neutron source. The MF corporation's bore hole neutron source will probably be used. It is nominally 1.688" in diameter, we assume a diameter of 2" on the inside of the target chamber due to wall thickness. The lower limit on pressures was chosen to be the atmospheric pressure in the mine, the upper limit is a governed by the pressure connectors can withstand. For the experimental setup Cajon fittings were used and capable of withstanding gauge

pressures as high as 100 psi. The capillary length was approximated to be 70 m. The radius of the decay chamber is limited by the size of the gate valve on the glove box.

Calculating the production rate of the gas calibration system is a multistep process. The first quantity to determine is the flow rate, Q, since this determines the amount of time the gas spends in the different components of the system. We have assumed that the tubing leading into the target chamber and out of the decay chamber will be sufficiently larger than the capillary between the target chamber and decay chamber so that they will not affect the flow. Thus the flow is dependant on the following system parameters: Ptgt, Cl, Cr, and Pdec. The flow rate is also dependant on the gas used, specifically the viscosity, η, in poise and the molar mass, MM, in grams. The flow rate, Q, can be modeled assuming fully developed flow of an ideal gas in a circular tube using fanning friction factors. Appendix B.2 explains the full derivation of the for expression the flow rate, in atm cm^3 s^{-1}, shown below.

$$Q = \left[\frac{f\_C (2Cr)^5 \left(P_{tgt}^2 - P_{dec}^2 \right)}{Cl \; 10^4} \left(\frac{2 \eta \; Cr}{R\_C \; MM} \right)^B \right]^{\frac{1}{B+2}}$$

The values of A and B were determined experimentally, as described in section 3. Values for A and B are given in table 2.2 below, the different values relate to different flow rate ranges. The proper values to use can easily be determined by choosing those that give the lowest flow rate.

Table 2.2, Flow Model Constants

A	B
1.26	-0.987
0.281	0.651
-1.50	-0.163

The production in the target chamber is dependent on the geometry as well as the specific gas used. Specifically the density ρ and cross section σ of the gas are needed. The same variable names are used for the geometry as described in table 2.1. The production rate can be calculated from:

$$dY = \frac{\sigma\ \rho\ dr\ \sin\theta\ d\theta\ d\phi}{4\pi}$$

For this geometry this expands to the equation below as explained in appendix B.1.

$$\begin{aligned} Y_T = {} & \frac{\sigma\rho(h-x)}{4}\left[\log\left(1+\left(\frac{R_2}{h-x}\right)^2\right) - \log\left(1+\left(\frac{R_1}{h-x}\right)^2\right)\right] \\ & - \frac{\sigma\rho R_1}{2}\left[\tan^{-1}\left(\frac{R_2}{h-x}\right) - \tan^{-1}\left(\frac{R_1}{h-x}\right)\right] \\ & + \frac{\sigma\rho}{2}(R_2 - R_1)\left[\tan^{-1}\left(\frac{R_2}{-x}\right) - \tan^{-1}\left(\frac{R_2}{h-x}\right)\right] \\ & - \frac{\sigma\rho x}{4}\left[\log\left(1+\left(\frac{R_1}{x}\right)^2\right) - \log\left(1+\left(\frac{R_2}{x}\right)^2\right)\right] \\ & - \frac{\sigma\rho R_1}{2}\left[\tan^{-1}\left(\frac{R_1}{-x}\right) - \tan^{-1}\left(\frac{R_2}{-x}\right)\right] \end{aligned}$$

Assuming complete mixing the mean time taken for a gas to pass through a container is:

$$t = \frac{PV}{Q}$$

For the Target chamber this becomes:

$$t_{tgt} = \frac{P_{tgt}\pi\left(R_2^2 - R_1^2\right)h}{Q}$$

While the gas is passing through the target chamber an amount of the produced gas will decay, the fraction that survives is given by:

$$e_{tgt} = \frac{1}{1+\frac{\tau_{tgt}}{\tau_{gas}}}$$

The mean life of the gas τ_{gas} is

$$\tau_{gas} = \frac{t_{1/2}}{\ln 2}$$

The $t_{1/2}$ for ^{16}N is 7.13 s so τ is 10.29 s (See appendix A for half and mean lives of other gases).

The transit time in the capillary tube is calculated by:

$$t_{cap} = \int_0^l \frac{P(x)}{Q} Area\ dx$$
$$= \frac{\pi(P_1+P_2)d^2 l}{8Q}$$

Thre pressure, P(x), is approximated to be simply the average pressure of the two ends of the capillary.

The fraction of radioactive gas that decays while passing through the capillary is

$$e_{cap} = \left(1 - e^{\frac{-\tau_{cap}}{\tau_{gas}}}\right)$$

Using the same time formula as for the target chamber and a spherical decay chamber,

$$\tau_{dec} = \frac{4\pi R_{dec}^3 P_{dec}}{3 Q}$$

then the fraction of the gas that does decay in the decay chamber is given by:

$$e_{dec} = \frac{1}{1 + \frac{\tau_{gas}}{\tau_{dec}}}$$

Thus the total efficiency of the system is given by: $e_{tot} = e_{tgt}\, e_{cap}\, e_{dec}$. The number of decays in the decay chamber per neutron produced by the neutron source is given by $Tp = Y_{tgt} \times e_{tot}$. The MF neutron source is capable of producing 10^7-10^8 N/s, the goal is to have a couple of hundred decays per second so that Y_{tot} must be at least 10^{-5}.

3. Experiment

To verify how the gas flows through a long capillary several samples were tested. The experimental setup is shown in figure 3.1, below. A single pressure gauge is used to measure the pressure at both ends of the capillary to reduce the systematic errors. A high pressure regulator was used on the gas cylinder to allow control above 60 gpsi. The MKS 30000, a mass flow

Figure 3.1, Experimental Setup

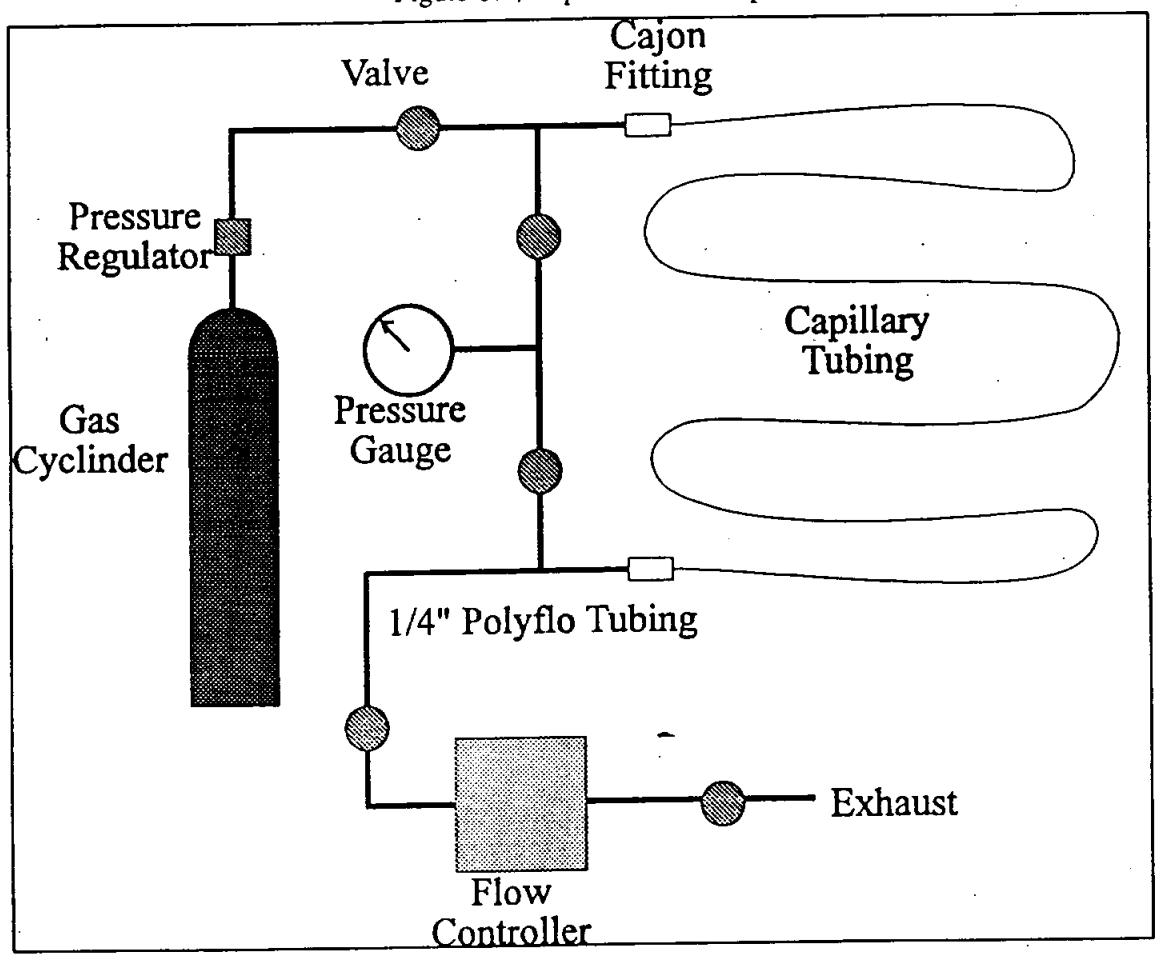

controller was used to control the flow through the system. The series of measurements were made by setting the pressure regulator and then varying the flow rate.

The analysis of the results followed standard engineering analysis methods involving the Reynolds number, Re, and the fanning friction factor, f_f. The derivation of the method is in appendix 2. The results of the measurements were used to produce a flow model from a graph of log(f) vs log(Re).

Figure 3.2, Gas flow in teflon capillary

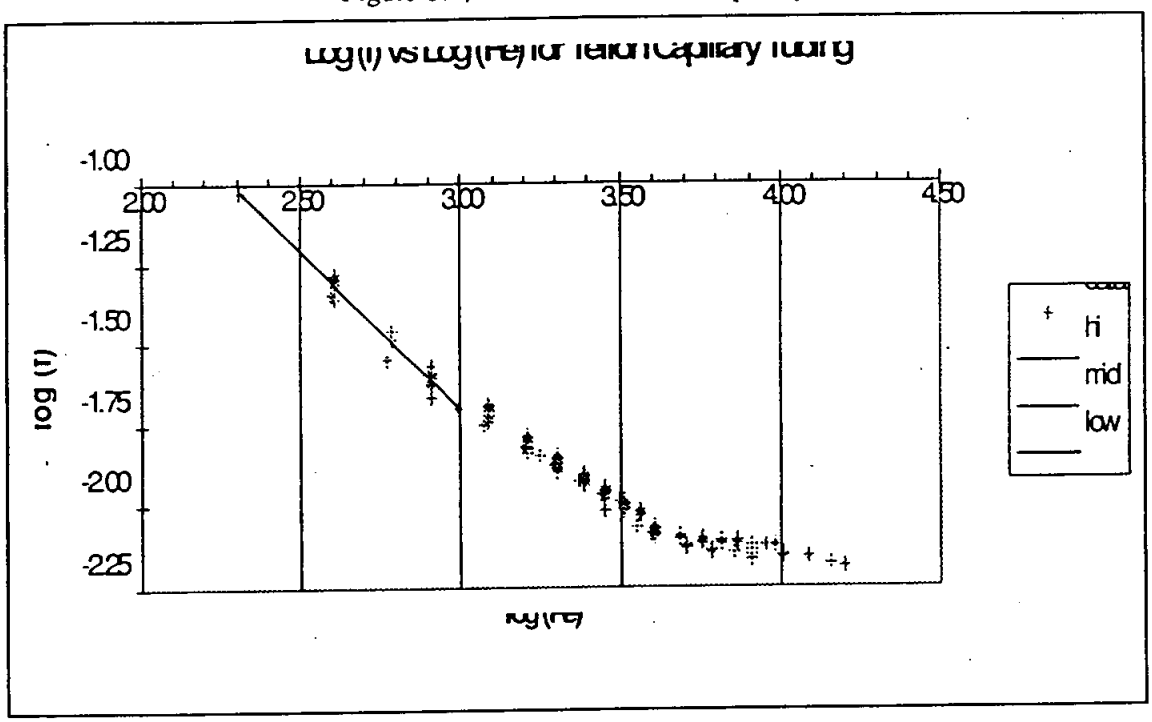

The results obtained were close to the theoretical values and the shape of the graph fits with theory. The data for the graph were fitted using three straight lines as shown in figure 3.1 above. The first line, for low flow, extends from no flow up to a Reynolds number of approximately 1000, the accepted range of laminar flow. Turbulent flow is a more empirical study but the results are close to the simplified case of a hydraulically smooth pipe.

A graph of Q vs P_1^2-P_2^2 is shown below for two different pieces of teflon capillary tube. The experimental results, the three fitted curves and the theoretical models are all shown. {1}

Figure 3.3, Teflon 4 Sample

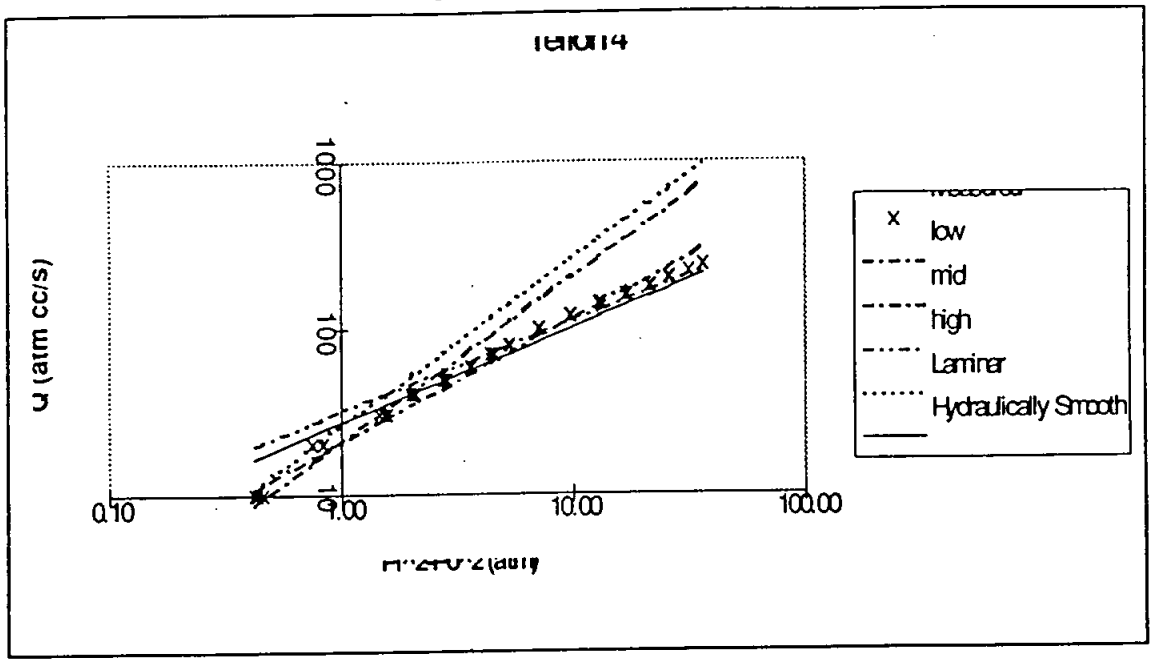

Figure 3.4, Teflon 1 Sample

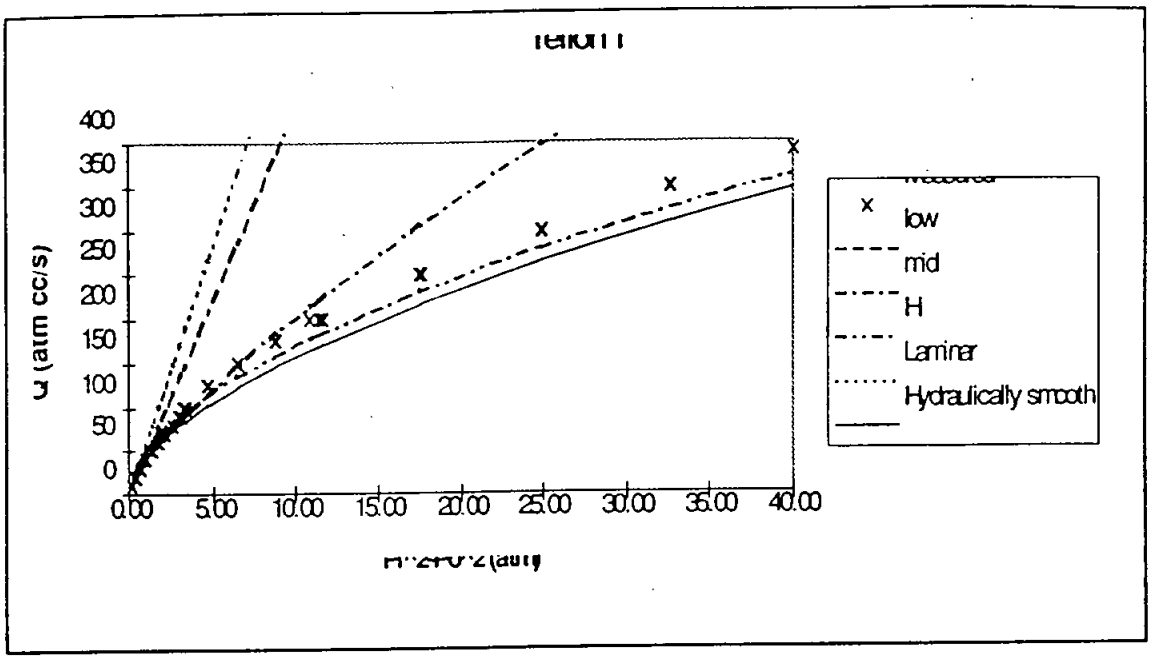

4. Programs

A collection of programs were written to optimize the system parameters to maximize the decay rate in the decay chamber. The programs were written in FORTRAN using the library subroutine STEPIT, written by J.P.Chandler, of Indiana University. Physics Dept. The program STEPIT was designed to find local minima of almost any real function of several variables {3}. STEPIT was designed to be used on functions that are continuous on a continuous domain and have continuous first derivatives.

The first program GOPTSTP finds the optimum configuration of the calibration system given the constraints on the parameters and starting values. There are two main sections to programs written with STEPIT. The first, found in GOPTSTUP.for, initializes all the constants and parameters needed to perform the optimization and calls STEPIT. The second is the subroutine FUNK, found in FUNKANU.for, which is called by STEPIT. This subroutine contains all the arithmetic to determine the production rate in the target chamber given the system variables. The subroutine FUNK contains the flow model created from the experimental work. Since STEPIT finds minima, FUNK returns $\frac{1}{p}$ to be minimized.

A second program, GOPTSRS.for, was written to test the validity of the solutions found by GOPTSTP. GOPTSRS takes a random starting point within the limits of the free parameters and records the optimized solution. The solutions can be checked to ensure that they are global maximums in the limited variable space rather than local maximums.

A third program, GOPTGR.for, was written to show how the system behaves as a function of the different system variables. The program fixes one free parameter at various values within its domain while the rest of the variables remain free and are re-optimized. This program outputs a table of the total production of the system and the gas flow rate as a function of one variable sweeping through its possible values. The output of this program is usually graphed.

5. Results

A summary of the output from GOPTSTP is listed below showing the optimum configuration of the calibration system for ^{16}N and ^{17}N gases. The units and explanation of the parameters can be found in table 2.1. The solid angle fraction (SAF) of the target chamber is included in the table.

Table 5.1, GOPTSTP Results

Parameter	^{16}N	^{17}N
Ptgt	5.00	5.00
R1	2.54	2.54
R2	6.29	6.49
h	10.19	10.57
xx	5.10	5.28
Cl	7000	7000
Cr	0.181	0.227
Pdec	3.31	2.99
Rdec	5.00	5.00
Q	422	829
Tp	1.80E-06	1.04E-6
SAF	0.55	0.55
Re	11100	17000
t_{tgt}	12.55	7.13
t_{cap}	7.06	5.47
t_{dec}	4.10	1.89
ε_{tgt}	0.45	0.46
ε_{cap}	0.50	0.40
ε_{dec}	0.29	0.24

The calibration system was optimized for both ^{17}N and ^{16}N gas. To test whether one set of chambers and capillary tube could be used for both the other gas was tested in the pre-optimized system. As table 5.2 shows only a small loss of efficiency was noted, an even smaller effect would occur if an average configuration was used.

Table 5.2, Gas Substitution Effect

	Total Production		Percent Difference
	Optimized	Substituted	
^{17}N	1.04E-06	9.07E-07	12%
^{16}N	1.80E-06	1.59E-06	13%

The results from goptgr are shown below for ^{16}N gas. The total production, Tp, and flow rate, Q, are both graphed to show when the system is limited by the flow rate.

Figure 5.1, Goptgr Results

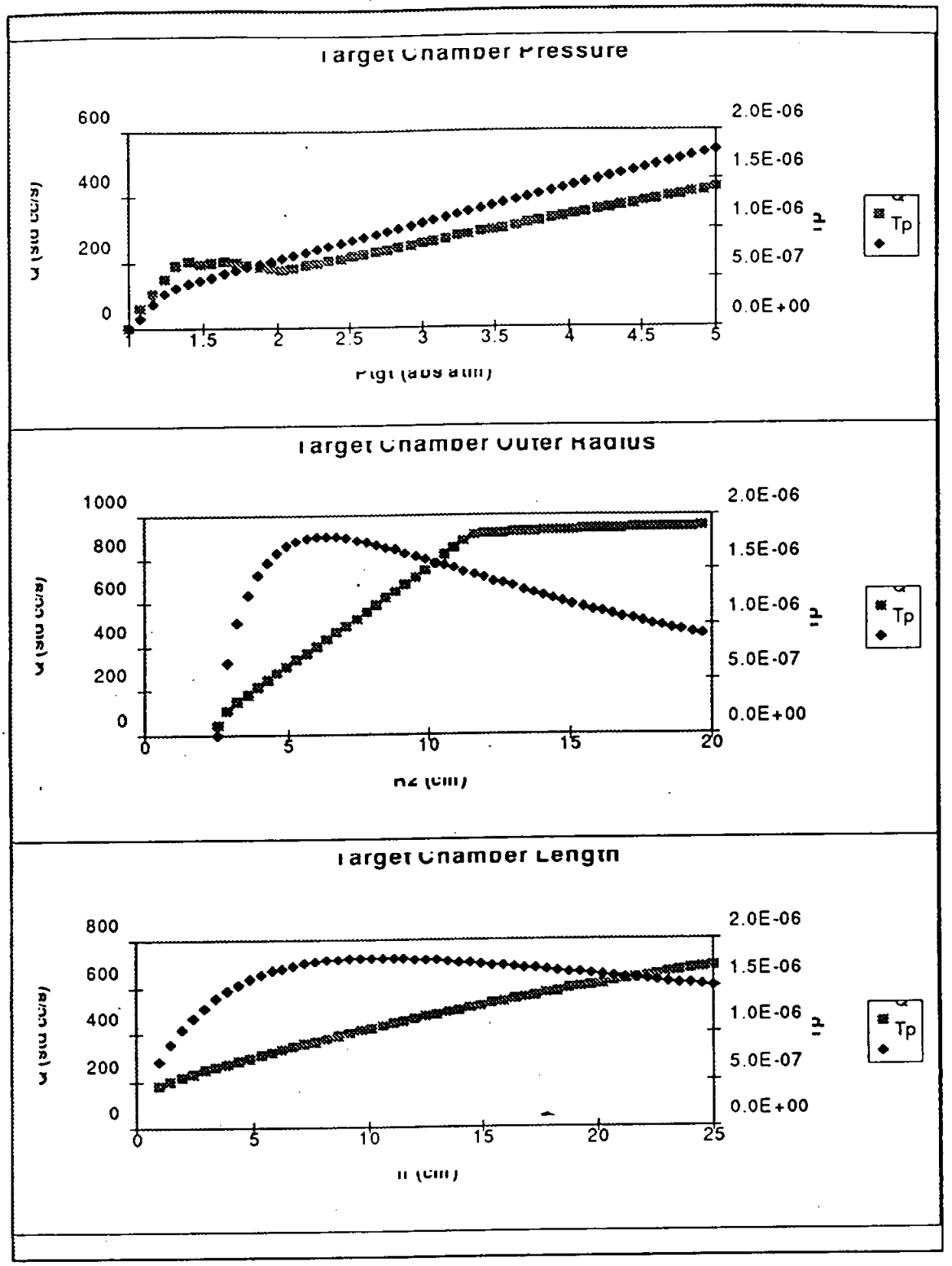

Figure 5.2, Goptgr Results

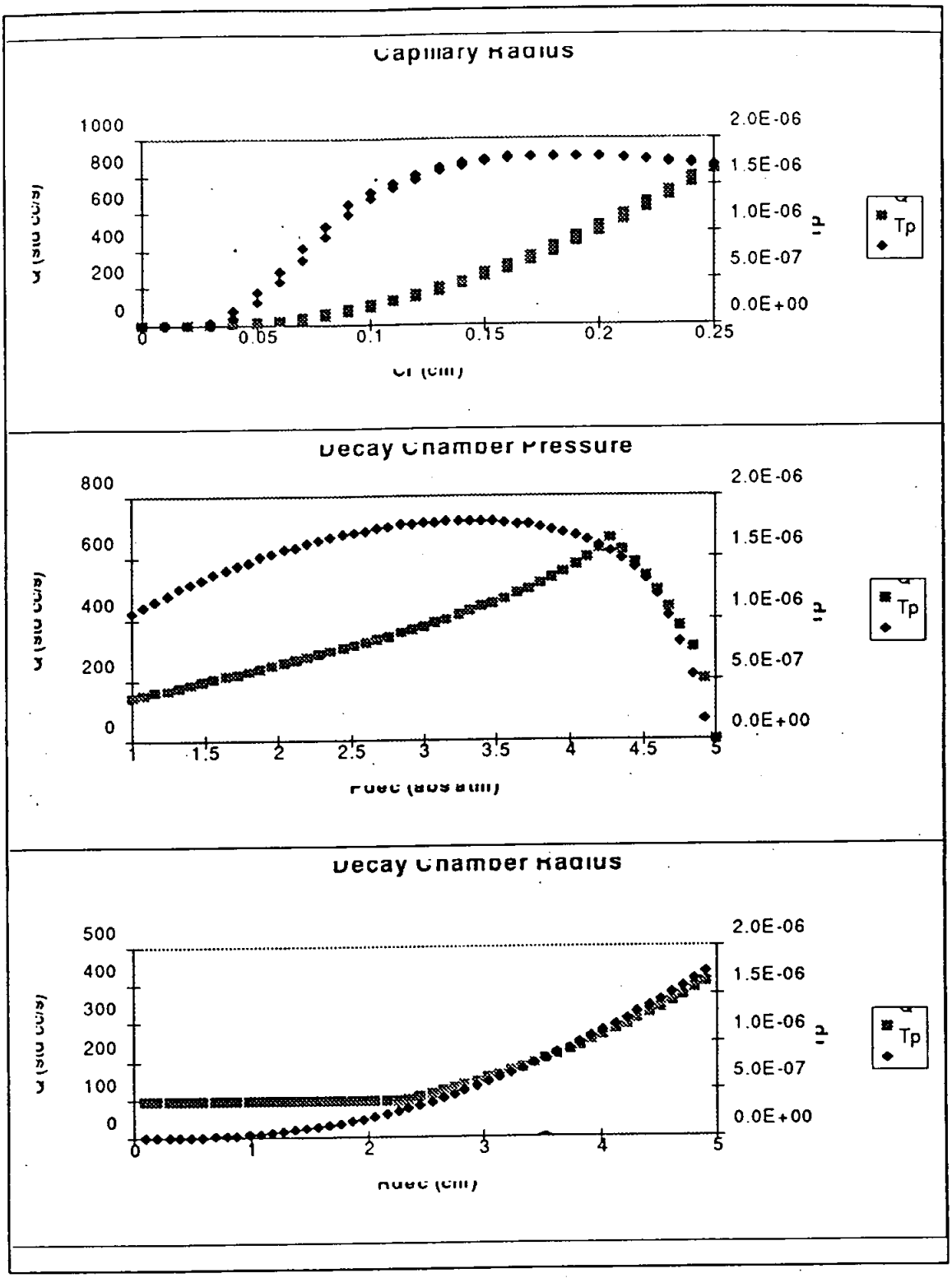

The graphs from goptgr show how the limits on the system are expressed. The target chamber pressure is optimized at the highest pressure possible to maximize the production rate. The increasing the size of the target chamber initially increases the production rate but eventually the production rate drops off. Increasing the size of target chamber always allows for a larger flow rate. The size of capillary tubing is a trade off between quick transport and the amount of gas transported. Similar to the target chamber the pressure of the decay chamber would be high except that a pressure difference is necessary to maintain the flow rate. The size of the decay chamber is as large as possible to allow the most gas to decay before exiting. This shows what modifications to the limits will provide the greatest gains in performance.

Teflon is the tubing of choice due to it's extreme inertness. Tubing is available in size increments of 1/32" inner diameter. Though distributors sell the tubing in standard length spools they are often several shorter pieces spliced together. A spliced tube is unacceptable for use between the outside of the glove box and the decay chamber since it will be threaded through a larger tube. Several companies and distributors were contacted to asses the cost and delivery time of tubing. The best company found was Johnston Industrial Plastics which can be contacted at 20 Fleeceline Road, Toronto, Ontario M8V 2K3, 1-800-268-2220. The catalog prices for flexible teflon tubing (virgin TFE) are approximately 7% below present costs. The table 5.3, below, lists possible capillary tubing that could be used with catalog prices. {11}

Table 5.3, Capillary Prices

Stock Number	I.D. (mm)	Wall (mm)	Price ($/foot)
9030-008-030	3.17	0.76	0.52
9030-012-030	4.76	0.76	0.79

To make the analysis of the calibration easier the preferred decay chamber geometry is a sphere. Due to the size of the gate valve on the glove box this limits the volume of the decay chamber. A problem this creates is that the residence time in the decay chamber can be comparable to the half life of the radioactive gas. The gas exiting the decay chamber will still be active and provide a signal which will be picked up by the detector. A possible solution to this problem is to have a cylindrical chamber which will allow a larger volume with the same diameter gate valve at the top of the acrylic vessel.

6. Design Specification

Given the results of the optimization it is now possible to fully specify the calibration source requirements for use with ^{16}N and ^{17}N gases. The major obstacle is to find suitable connectors for the teflon capillary. The cajon fittings worked well for the experiment, but a system where the capillary cannot slide out of the fitting is necessary for a permanent installation. Flared fittings are used for larger diameter tubing but are not commercially available for the size of capillary used in this system. It may be possible to produce a fitting of the same design for the small diameter tubing.

A partial list of the design requirements of the calibration system has been developed. This list assumes that ^{8}Li will also be used as a calibration source. The main components of calibration system are: the neutron generator, control electronics for the neutron generator, target chambers, fast and slow neutron flux monitoring equipment, shielding, an aerosol generator, gas supplies, gas flow regulation/measurement equipment, the capillary and the target chambers. {10}

At present the A-320 Probe Neutron Generator produced by MF Physics Corporation is the most likely neutron source. This generator is a 88" long, 1 11/16" diameter cylinder with a nominal output of $1x10^{8}$ n/sec. The control electronics for this neutron generator can be placed in a standard rack. {7}

The final design should incorporate a method of changing target chambers for different calibrations. Both ^{17}N and ^{16}N will probably use the same target chamber since there is little loss of performance. The target chambers will be annular such that the neutron source can be slid into the centre.

A scintillator will be used for the fast neutron flux monitor close to neutron generator. The monitor will be measuring 14 MeV neutrons. A slow neutron flux monitor above pit is

required to monitor the neutron hazard levels to personnel from thermal neutrons. The monitoring electronics for the neutron flux should fit in a NIM crate in the same rack as the neutron generator electronics.

The best candidate for the shielding is water due to the fire hazard of paraffin or borated plastic. Water will also alow for easier changing of target chambers.

Gas supplies are needed for each calibration source. For $^{16}O_2$ and ^4He a high pressure dewar with controlled heater or a gas cylinder with regulator could be used. The gas expelled from the decay chamber must be properly exhausted. For ^{17}N gas a recirculating system will be used, a collection system is needed for when this calibration is not in use as well as a way of checking the gas integrity of the system.

The aerosol generator consists of an oven containing NaCl within the oven tube and accessories to control the temperature and cool the gas upon exit.

The capillary can easily be routed from the target chamber to the decay chamber along existing pipes or in cable trays because of it's flexibility and small diameter.

The Calibration system must be capable of meeting the following criterion. An adequate flux of neutrons is needed to provide the following decay rates: 10-100 d/s for ^{16}N, 10-30 d/s for ^{17}N and at least 1 d/s for ^8Li. The neutron source must be sufficiently shielded to provide a safe working environment for the operator and others in the observatory. The Neutron flux must be monitored both at the target chamber, for the calibration, and outside the shielding to guarantee worker safety. All materials used in the calibration system must have low background levels to maintain the background of the observatory. All equipment must also meet the standards necessary to be used in the mine.

References

1. Atta, V., "Vacuum Science and Engineering"; McGraw-Hill Book Company, 1965.

2. Bird,R.B., Stewart, W.E., Lightfoot, E.N., "Transport Phenomena"; John Wiley and Sons, New York, 1960.

3. Chandler, J.P., "STEPIT Manual"; Indiana University Physics Department

4. Choi, M, Private Communication Oct-Nov 1994

5. Earle, E.D., "Observing the Sun from Two Kilometers Underground"; AECL Research.

6. Ewan, G.T. "Sudbury Neutrino Observatory" in Frontiers of Neutrino Astrophysics; Universal Academy Press Inc, 1993

7. MF Physics Corporation, "The A-320 Probe Neutron Generator"

8. Sur, B. et al., "^{16}N : A Calibration Source for SNO"; AECL Research.

9. Sur, B., "Signals, Backgrounds and Calibrations in the Sudbury Neutrino Observatory"; AECL Research, 1994.

10. Sur, B. Private Communication Sept-Dec 1994

11. Johnston Industrial Plastic Catalog

Appendix

A. Physics Constants and Conversion Factors

B. Derivations

1. Target Chamber Production
2. Gas Flow in Capillary Tubing

C. Program Listings

Physical Constants

Substance	$t_{1/2}$ (s)	τ(s)	σ(mb)
^{17}N	4.173	6.02	28
^{16}N	7.13	10.24	35
^{8}Li	0.838	1.21	

Substance	Viscosity (poise)
air (20°C)	182.9×10^{-6}
O_2 (0°C)	191.0×10^{-6}
N_2 (0°C)	166.6×10^{-6}
He (0°C)	186.9×10^{-6}

Conversion Factors

poise = dyne s / cm^2

1 N = 1 kg m / s^2 = 10^5 dynes

1 atm = 1.013×10^6dyne s / cm^2

1 barnnes = 10^{-24} cm^2

$$1 \frac{dynes}{cm^2} \frac{cm^3}{s} = 9.872 \times 10^{-7} \frac{atm\ cm^3}{s}$$

Derivations

1. Target Chamber Production

$$dY = \frac{\sigma \rho \, dr \sin\theta \, d\theta \, d\phi}{4\pi}$$

Due to the cylindrical symmetry this simplifies to

$$dY = \frac{\sigma \rho}{2} dr \sin\theta \, d\theta$$

The integration of dY is broken into three parts as shown in the cutaway drawing of the target chamber below.

Figure XXXX. Cross Section of target chamber.

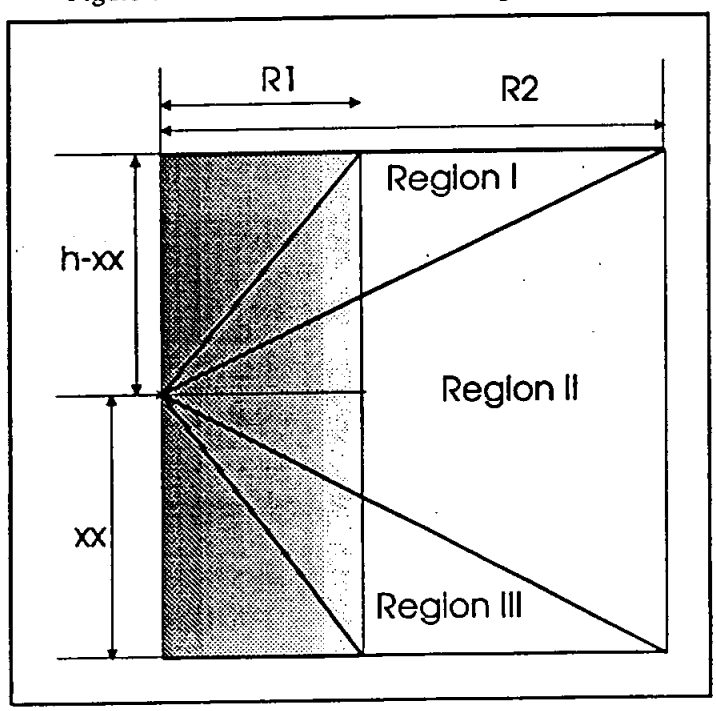

Region I.

$$\tan^{-1}\left(\frac{R_1}{h-x}\right) < \theta < \tan^{-1}\left(\frac{R_2}{h-x}\right)$$

$$\sin\theta = \frac{R_1}{r} \qquad \cos\theta = \frac{h-x}{r}$$

r goes from to

$$r = \frac{R_1}{\sin\theta} \qquad r = h - x\frac{f}{\sin\theta}$$

So that

$$Y_1 = \frac{\sigma\rho}{2}\int_{\tan^{-1}\left(\frac{R_1}{h-x}\right)}^{\tan^{-1}\left(\frac{R_2}{h-x}\right)}\left(\frac{h-x}{\cos\theta} - \frac{R_1}{\sin\theta}\right)\sin\theta\, d\theta$$

$$= \frac{\sigma\rho}{2}\int\left[(h-x)\tan\theta - R_1\right]d\theta$$

$$= \frac{\sigma\rho}{2}\left|\frac{(h-x)}{2}\log(1+\tan^2\theta) - R_1\right|_{\tan^{-1}\left(\frac{R_1}{h-x}\right)}^{\tan^{-1}\left(\frac{R_2}{h-x}\right)}$$

$$Y_1 = \frac{\sigma\rho(h-x)}{4}\left[\log\left(1+\left(\frac{R_2}{h-x}\right)^2\right) - \log\left(1+\left(\frac{R_1}{h-x}\right)^2\right)\right]$$

$$- \frac{\sigma\rho R_1}{2}\left[\tan^{-1}\left(\frac{R_2}{h-x}\right) - \tan^{-1}\left(\frac{R_1}{h-x}\right)\right]$$

Region II

$$\tan^{-1}\left(\frac{R_2}{h-x}\right) < \theta < \tan^{-1}\left(\frac{R_2}{-x}\right)$$

$$\sin\theta = \frac{R_1}{r} \qquad \sin\theta = \frac{R_2}{r}$$

r goes from to

$$r = \frac{R_1}{\sin\theta} \qquad r = \frac{R_2}{\sin\theta}$$

So that

$$Y_{II} = \frac{\sigma\rho}{2}\int_{\tan^{-1}\left(\frac{R_1}{h-x}\right)}^{\tan^{-1}\left(\frac{R_2}{-x}\right)} \frac{R_2 - R_1}{\sin\theta}\,\sin\theta\,d\theta$$

$$= \frac{\sigma\rho}{2}(R_2 - R_1)\left[\tan^{-1}\left(\frac{R_2}{-x}\right) - \tan^{-1}\left(\frac{R_2}{h-x}\right)\right]$$

Region III

$$\tan^{-1}\left(\frac{R_2}{-x}\right) < \theta < \tan^{-1}\left(\frac{R_1}{-x}\right)$$

$$\cos\theta = \frac{-x}{r} \qquad \sin\theta = \frac{R_1}{r}$$

r goes from $r = \frac{-x}{\cos\theta}$ to $r = \frac{R_1}{\sin\theta}$

So that

$$Y_{III} = \frac{\sigma\rho}{2}\int_{\tan^{-1}\left(\frac{R_1}{-x}\right)}^{\tan^{-1}\left(\frac{R_2}{-x}\right)} \left(\frac{-x}{\cos\theta} - \frac{R_1}{\sin\theta}\right)\sin\theta\,d\theta$$

$$= \frac{\sigma\rho}{2}\int(x\tan\theta + R_1)d\theta$$

$$= \frac{-\sigma\rho x}{2}\log(1 + \tan^2\theta) + R_1\theta\Big|_{\tan^{-1}\left(\frac{R_2}{-x}\right)}^{\tan^{-1}\left(\frac{R_1}{-x}\right)}$$

$$Y_{III} = \frac{-\sigma\rho x}{4}\left[\log\left(1 + \left(\frac{R_1}{x}\right)^2\right) - \log\left(1 + \left(\frac{R_2}{x}\right)^2\right)\right]$$

$$- \frac{\sigma\rho R_1}{2}\left[\tan^{-1}\left(\frac{R_1}{-x}\right) - \tan^{-1}\left(\frac{R_2}{-x}\right)\right]$$

The Total Production in the target chamber is:

$$
\begin{aligned}
Y_T = {} & \frac{\sigma\rho(h-x)}{4}\left[\log\left(1+\left(\frac{R_2}{h-x}\right)^2\right)-\log\left(1+\left(\frac{R_1}{h-x}\right)^2\right)\right] \\
& -\frac{\sigma\rho R_1}{2}\left[\tan^{-1}\left(\frac{R_2}{h-x}\right)-\tan^{-1}\left(\frac{R_1}{h-x}\right)\right] \\
& +\frac{\sigma\rho}{2}(R_2-R_1)\left[\tan^{-1}\left(\frac{R_2}{-x}\right)-\tan^{-1}\left(\frac{R_2}{h-x}\right)\right] \\
& -\frac{\sigma\rho x}{4}\left[\log\left(1+\left(\frac{R_1}{x}\right)^2\right)-\log\left(1+\left(\frac{R_2}{x}\right)^2\right)\right] \\
& -\frac{\sigma\rho R_1}{2}\left[\tan^{-1}\left(\frac{R_1}{-x}\right)-\tan^{-1}\left(\frac{R_2}{-x}\right)\right]
\end{aligned}
$$

2. Gas Flow in Capillary Tubing

The model of gas flow in capillary tubing was made based on friction factors for fully developed flow in circular tubes {2,4}. The gases were assumed to be ideal. All the variables have the same units and definitions as given in the body of the paper.

Starting with the definition of the dimensionless fanning friction factor

$$f = \frac{R}{2L}\frac{P_1 - P_2}{\frac{1}{2}\rho\langle v\rangle^2}$$

The average density, ρ, is derived from the ideal gas state law as shown below.

$$PV = nRT$$

$$\rho = \frac{n}{V} = \frac{P}{RT}$$

$$\rho\left(\frac{g}{cm^3}\right) = \frac{P_1 + P_2}{2}\frac{M}{R_o T}$$

The flow rate is converted from std cc s^{-1} to g s^{-1} by the following calculation.

$$Q\left(\frac{g}{cm^3}\right) = \frac{Q\left(\frac{std\ cc}{s}\right) MM\left(\frac{g}{mol}\right)}{22415\left(\frac{cc}{mol}\right)}$$

The velocity of the gas can be calculated as follows.

$$Q = \rho\langle v\rangle A$$

$$\rho\langle v\rangle = \frac{Q}{A}$$

$$\rho\langle v\rangle^2 = \frac{Q^2}{\rho A^2}$$

The cross-sectional area of the capillary, A, is given by

$$A = \pi\, cr^2$$

Substituting all these into the definition of the fanning friction factor gives

$$f = \frac{f\_C\ (2R_c)^5\ (P_i^2 - P_o^2)}{L_c\ Q^2}$$

Where all the constants have been grouped together in f_C.

$$f\_C = \frac{(22\ 415\ \pi)^2 \times 1.0133 \times 10^6}{64\ R_o\ T\ M}$$
$$= 1.14 \times 10^8$$

The Reynolds number, a measure of the turbulence of the flow, is defined by the equation below.

$$Re = \frac{D\rho\langle v\rangle}{\eta}$$

Using the same substitutions as above this simplifies to,

$$Re = \frac{ReC\ Q\ MM}{2\ \eta\ R_c}$$

$$ReC = \frac{4}{\pi\ 22415}$$
$$= 5.68 \times 10^{-5}$$

Variable	Unit
Q	std cc/s
M	g/mol
η	poise
L, R	cm
P_i, P_o	abs atm.

A plot of log(f) vs log(Re) was made as per standard practice. Three linear fits were made to the data providing a formula of the form:

$$\log(f) = A + B \log(Re)$$
$$f = 10^{A} Re^{B}$$

The specific values of A and B obtained are in table 2.2.

Substitution of f and Re gives:

$$\frac{f C (2R_c)^5 (P_i^2 - P_o^2)}{L_c Q^2} = 10^{A} \left(\frac{ReC\ Q\ MM}{2\ \eta\ R} \right)^{B}$$

Which can be simplified to:

$$\frac{f C (2R_c)^5 (P_i^2 - P_o^2)}{L_c\ 10^{A}} \left(\frac{2\ \eta\ R_c}{R C\ MM} \right)^{B} = Q^{B+2}$$

The final result gives the flow rate as a function of all the variables of the system.

$$Q = \left(\frac{f C (2R_c)^5 (P_i^2 - P_o^2)}{L_c\ 10^{A}} \left(\frac{2\ \eta\ R_c}{R C\ MM} \right)^{B} \right)^{\frac{1}{B+2}}$$

Program listings

GOPTSTP.for

GOPTSRS.for

GOPTGR.for

FUNKANU.for

GOPTSTUP.for

STEPIT.for

Program listings

GOPTSTP.for

GOPTSRS.for

GOPTGR.for

FUNKANU.for

GOPTSTUP.for

STEPIT.for